for all k except those close to 0 or n.

If, on the other hand, we fix the zeroth monomer at the origin, but for the nth monomer require only that $z_n = l$, it is found that

$$m_k = \frac{b^2}{3s} \frac{\sinh ns - \sinh (n - 2k)s}{\cosh ns} \quad \text{(A9)}$$

which for large values of ns is again almost flat at level $m_k = b/w$, except near $k = 0$ and near $k = n$, but this time m_k increases near $k = n$ to become equal to twice the average value in the rest of the tube. The same is true for m_0 when we require only that the zeroth monomer is in the plane $z = 0$. This explains why the average in eq A4 is twice as large as that in eq A8.

Finally, it may be mentioned that more general results, when $ns \gg 1$, can be obtained also for arbitrary values of s, for example

$$m_k = \frac{b}{w} \left\{1 + \left(\frac{bw}{6}\right)^2\right\}^{-1/2} \quad \text{(A10)}$$

but it falls outside the scope of the present work to pursue this case further.

References and Notes

(1) A. S. Lodge, "Elastic Liquids", Academic Press, New York, 1964.
(2) M. Doi and S. F. Edwards, *J. Chem. Soc., Faraday Trans. 2*, **74**, 1789 (1978).
(3) M. Doi and S. F. Edwards, *J. Chem. Soc., Faraday Trans. 2*, **74**, 1802 (1978).
(4) M. Doi and S. F. Edwards, *J. Chem. Soc., Faraday Trans. 2*, **74**, 1818 (1978).
(5) M. Doi and S. F. Edwards, *J. Chem. Soc., Faraday Trans. 2*, **75**, 38 (1979).
(6) P. G. de Gennes, *J. Chem. Phys.*, **55**, 572 (1971).
(7) G. Marrucci and B. de Cindio, *Rhenol. Acta*, in press.
(8) M. Fukuda, K. Osaki, and M. Kurata, *J. Polym. Sci., Part A*, **13**, 1563 (1975).
(9) J. Klein, *Macromolecules*, **11**, 852 (1978).
(10) J. P. Cotton, D. Decker, H. Benoit, B. Farnoux, J. Higgins, G. Jannink, R. Ober, C. Picot, and J. Des Cloizeaux, *Macromolecules*, **7**, 863 (1974).
(11) M. Daoud, J. P. Cotton, B. Farnoux, J. Jannink, G. Sarma, H. Benoit, R. Duplessix, C. Picot, and P. G. de Gennes, *Macromolecules*, **8**, 804, (1975).
(12) S. F. Edwards, quoted in ref 2.
(13) H. M. Laun and H. Münstedt, *Rhenol. Acta*, **17**, 415 (1978).
(14) R. L. Ballman, *Rheol. Acta*, **4**, 137 (1965).
(15) S. Chandrasekhar, *Rev. Mod. Phys.*, **15**, 1 (1943).
(16) Equation A5 of ref 3 contains a misprint in the second exponential term.

A Neutron Scattering Study of the Chain Trajectory in Isotactic Polystyrene Single Crystals

Jean-Michel Guenet

Centre de Recherches sur les Macromolécules (CNRS), 67083 Strasbourg-Cedex, France.

Received September 19, 1979

ABSTRACT: The trajectory of a chain in well-charcterized isotactic polystyrene (IPS) single crystals has been examined by means of small-angle neutron scattering (SANS). Both the variation of mean dimensions with molecular weight and asymptotic behavior have been studied. The results are consistent with a sheet-like conformation along the 330 crystallographic plane.

Small-angle neutron scattering (SANS) has recently been used extensively to study the trajectory of a chain in bulk semicrystalline polymer. The first results obtained on polyethylene samples[1,2] rapidly quenched from melt to room temperature were compatible with those of the Flory model for which only small portions of the chain are incorporated sequentially in several crystalline lamellae. However, from the recent studies that we performed on semicrystalline isotactic polystyrene[3] (IPS), we have concluded that the conformation depends strongly on the chain mobility in the original amorphous medium. As suggested by Flory,[4] two parameters can be considered: the long relaxation time τ_m of the chains in the amorphous state and the time τ_p needed for the crystalline growth front to go through the dimension of one amorphous chain. This last parameter is evaluated according to

$$\tau_p \sim R_g/G \quad (1)$$

where R_g is the radius of gyration of the amorphous macromolcules and G the radial crystalline growth rate. In bulk polyethylene the relation $\tau_p << \tau_m$ is always valid, and therefore Flory[4] predicted that the thermal motions of units of the chain can affect only limited arrangements leading to a globally Gaussian chain made of amorphous subunits and small crystallized portions. In contrast, for IPS crystallized at 180 °C from the amorphous state the relations $\tau_m \sim \tau_p$ and $\tau_m >> \tau_p$ can be easily obtained by only using **H** matrices of different molecular weights.[5] SANS experiments[3] revealed indeed the existence of a schematic conformation possessing a long crystallized sequence folded along the 330 plane with two amorphous wings for the first situation ($\tau_m \sim \tau_p$) and the Flory type conformation for the second situation ($\tau_m >> \tau_p$). These results were supported both by the evolution of the mean dimensions with crystallinity and by the asymptotical scattering behavior.

As a consequence, one can reasonably expect a total incorporation of the chain forming a slab along the 330 crystallographic plane in self-seeded monocrystals grown from dilute solutions. Indeed, the long relaxation time in solution is rather small whereas the growth rate of single crystals is slow leading to $\tau_m \ll \tau_p$. Such an assumption has been confirmed by Sadler and Keller[6] from SANS experiments on polyethylene. For IPS, Keith, Vadimsky, and Padden[7] suggested a similar model by taking into account the regular hexagonal shape of the single crystals as seen by electron microscopy.

It is the purpose of this paper to describe SANS experiments carried out on IPS single crystals in order to confirm the earlier interpretation.

Experimental Section

1. **Materials.** Both hydrogenated (IPSH) and deuterated (IPSD) polymers were synthesized according to the Natta me-

0024-9297/80/2213-0387$01.00/0

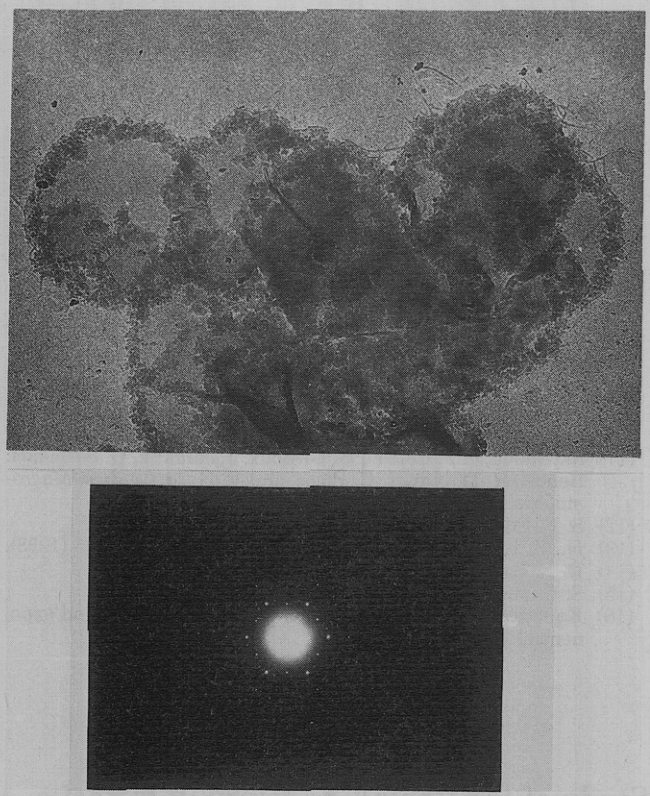

Figure 1. (a, top) Electron microscopy picture of a cluster of IPS single crystals of approximative size 2 μm. (b, bottom) Diffraction pattern of an IPS single crystal obtained from electon microscopy.

thod.[8] A detailed description of synthesis, purification, fractionation, and tacticity measurements achieved on these polymers is reported in a previous paper.[9] Experiments were carried out with IPSD samples of weight average molecular weights ranging from 9.5×10^4 to 5×10^5 of narrow polydispersities (see Table I). By using a hydrogenated matrix of molecular weight $M_w = 8.5 \times 10^5$ ($M_w/M_n \sim 3$), we prepared solid state solutions of about 1% in D species by dissolving them in boiling chlorobenzene and then coprecipitating them into an excess of methanol by dropwise addition. Crystallizations from 1.5% solutions in dibutyl phthalate were carried out, without stirring, in tubes immersed in an oil bath held at a constant temperature, $T_c = 130$ °C (±0.5 °C). The crystallized material was recovered by slight centrifugation and then washed thoroughly with methyl ethyl ketone in order to remove the uncrystallized chains. The specimens were then suspended in a 2% toluene solution of protonated atactic polystyrene of broad molecular weight distribution in order to fill up the possible holes and to facilitate the compression process. Disk-shaped samples of about 0.8 mm thickness and 1.2 cm diameter were obtained by compression molding at 140 °C so as to produce translucent material and to minimize voids. At this temperature the structure of the single crystals is almost unaffected.[10]

It must be emphasized that no mats were obtained under these circumstances but only aggregates of small disoriented grains containing stacked lamellae.

2. Structural and Thermal Characterization of the Single Crystals. From electron microscopy, a bright field picture (Figure 1a) and a diffraction pattern (Figure 1b) show that we are dealing with classical IPS single crystals. The thickness of lamellae $l_c = 78 \pm 15$ has been determined by shadowing the lamellae with Pt/C and coating them with carbon. DSC measurements performed on a Perkin-Elmer DSC2 with approximatively 5 mg of material placed in a hermetically sealed sample pan lead to a melting temperature of $T_m = 207$ °C for a heating rate of 20 °C/min. As reported by Lemstra et al.,[11] two melting endotherms were obtained (Figure 2). From the melting areas a degree of crystallinity $x = 0.74$ has been deduced by using the theoretical value $\Delta H_{IPS} = 8.6\ 10^8$ erg/cm^3 calculated for a perfect crystal[12] and calibrating the apparatus with indium ($\Delta H_{In} = 6.9$ cal/g). From small-angle X-ray scattering, the long-spacing distance d

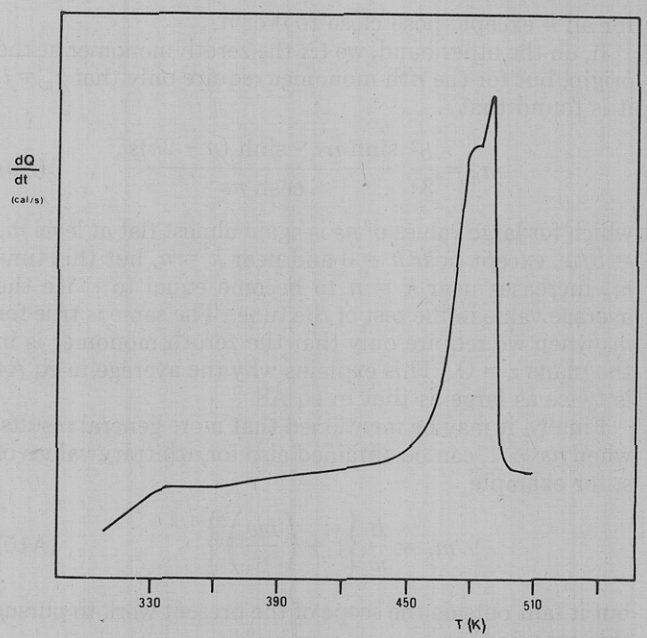

Figure 2. DSC melting endotherms of IPS single crystals grown at 130 °C in dibutyl phthalate. The heating rate was 20 °C/min.

= 94 Å has been determined. Approximating the crystallinity x found by means of DSC to the linear crystallinity $X_L = l_c/d$, one obtains a lamellar thickness of

$$l_c = 67 \pm 4 \text{ Å}$$

3. Neutron Scattering. The experiments reported here have been carried out at the ILL high flux reactor in Grenoble (France) on D11 and D17 cameras.[13] The scattering vector $q = (4\pi/\lambda) \sin(\theta/2)$ ranged from $5 \times 10^{-3} \leq q$ (Å^{-1}) $\leq 1.5 \times 10^{-2}$ for D11 and $10^{-2} \leq q \leq 6.5 \times 10^{-2}$ for D17. For the two cameras a mechanical monochromator was employed providing a wavelength distribution characterized by a width at half-height $\Delta\lambda/\lambda$ of about 10%.

All the results have been treated with an H–water spectrum for calibration, allowing the cross-checking of the data obtained with D11 and D17. Furthermore, a reference sample (IPSD with $M_w = 5 \times 10^5$ dispersed in APSH) with a well-defined scattering envelope[14] has been used in order to obtain accurate values of molecular weights.

Neutron scattering by crystalline polymers cannot be regarded as a simple problem. In IPS single crystals where clustering does not occur (see below), three entities are effectively present in the sample: the amorphous material located mainly in the junction loops; the crystalline material; and the microvoids arising principally from an insufficient compression of the sample.

For this last point, comparing the percentages of transmission of the incident neutron beam for both compressed molded single crystal and amorphous bulk as a function of sample thickness, we have obtained the same variation which indicates that microvoids can be ignored.

On the other hand, Figure 3 shows that the protonated background (S.C.) exhibits a pronounced upturn at small q compared to an amorphous matrix. This appearance of coherent scattering from a hydrogenated background is probably due to the significant density fluctuations arising from the existence of large crystalline domains separated by the amorphous continuum. However, the excess of intensity $I(q)$ scattered by the isolated labeled chains in the protonated surrounding can be obtained by subtracting from the blend signal $I_T(q)$ a blank signal $I_o(q)$ provided by a pure hydrogenated matrix prepared under the same conditions. We have shown in a previous paper[3] that for IPS, $I_o(q)$ does not need to be rescaled since it is a very good approximation for the intensity scattered by the hydrogenated chains in the blend for low concentrations in D species ($C_D \sim 1\%$).

Results

SANS experiments allow the investigation of correlation distances ranging from the overall dimension to the statisical unit of a labeled chain. Generally, one distinguishes

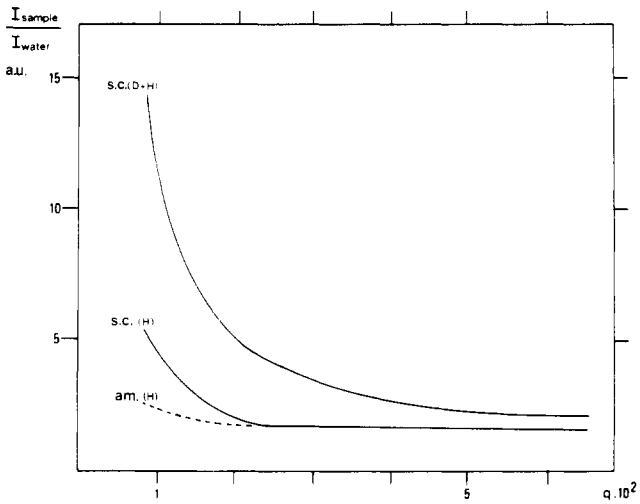

Figure 3. Intensities in arbitrary units normalized by H–water spectrum: [am. (H)] = amorphous matrix; [S.C. (H)] = single crystal blank, [S.C. (H+D)] = single crystal sample containing about 1% of D species.

Table I

M_w	M_w/M_n	R_g
5×10^5	1.2	330 ± 30
2.5×10^5	1.15	221 ± 20
1.5×10^5	1.13	110 ± 10
9.5×10^4	1.13	78 ± 6

two ranges of scattering vectors: the Guinier range ($qR_g \ll 1$) where the scattered intensity $I(q)$ can be approximated by

$$I(q) \sim 1 - \frac{q^2 R_g^2}{3} \tag{2}$$

and the asymptotic range ($qR_g \gg 1$) in which the pair correlations related to shorter distances of the conformation are predominant. Generally, $I(q)$ reduces to

$$I(q) \sim 1/q^n \tag{3}$$

where n is an exponent characteristic of the conformation. One has to note that in this range different specific behaviors can be successively present defining a crossover scattering vector q^*.[15]

1. Guinier Range. For IPS single crystals, the variation of the mean dimensions R_g as a function of weight average molecular weight of the tagged species leads from results listed in Table I to the following relation calculated with a mean least-squares method:

$$R_g \sim M^{0.91} \tag{4}$$

Results of Table I show an appreciable increase of R_g more marked for the highest molecular weights. The plots log R_g vs. log M_w for the data relative to single crystals and amorphous samples illustrate this difference (Figure 4). Such an increase cannot in our case be attributed to the clustering of labeled chains as reported often for polyethylene.[1,6] Indeed, Figure 5 shows plainly that the Zimm representations associated with single crystals and the reference sample (note in the two cases $M_{wIPSD} = 5 \times 10^5$) lead to the same extrapolations for $q = 0$. This shows clearly the nonexistence of aggregates of tagged chains in IPS monocrystals. It seems interesting to mention that whatever the treatment achieved to crystallize IPS, in no case do we observe any segregation of the D species.[3]

2. Asymptotic Range. The behavior of the samples at high q has been examined with the D17 camera and

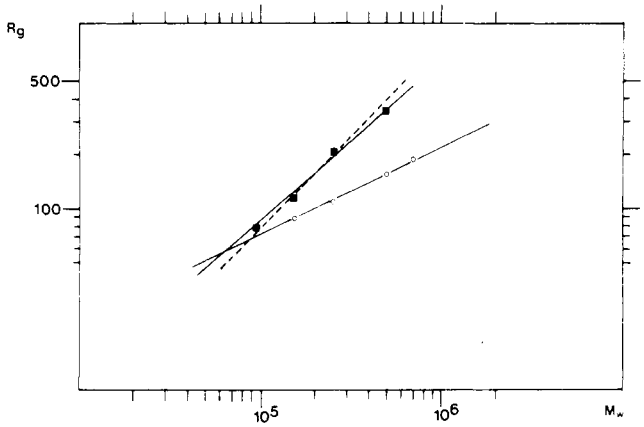

Figure 4. Plot of log R_g vs. log M_w: (■) Tagged chains in single crystal, (o) amorphous sample molded at 250 °C (previous results available in ref 14). The dotted line stands for theoretical variations derived from relation 5 with $(\bar{l}^2)^{1/2} = 12.6$ Å.

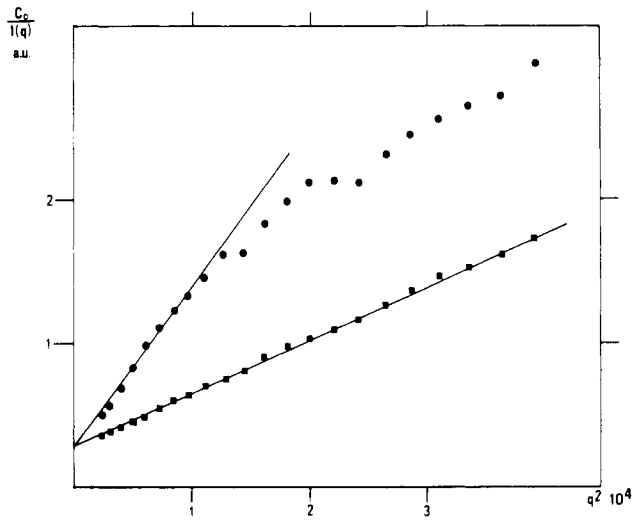

Figure 5. Zimm plot $C_D/I(q)$ vs. q^2. The circles stand for single crystal sample and the squares for amorphous sample. In the two cases $M_{wIPSD} = 5 \times 10^5$. One notices for the single crystal sample the departure from the Guinier regime to the first asymptotical regime.

leads to the results plotted in Figure 6a according to a Kratky plot ($q^2I(q)$ vs. q) and in Figure 6b using a double logarithmic scale. These two different representations reveal a crossover occurring at $q^* = 2.75 \times 10^{-2}$ Å^{-1}. For $q < q^*$, $I(q)$ behaves like q^{-1}, and for $q > q^*$, $I(q)$ behaves like q^{-2}.

The results will not be discussed in terms of the different types of chain incorporation into the crystalline lamella.

Discussion

In single crystals, the chain can thread through the lamella in two ways as shown in Figure 7. Thus we are dealing with the sheet-like (SL) and the switch-board (SB) models for which we have given[16] a general expression of the mean dimensions as a function of molecular weight:

$$\bar{R}_g^2 = \bar{r}_e^2 + x^{2\nu} \left(\frac{M}{M_r} \right)^{2\nu} \frac{\bar{l}^2}{(1 + 2\nu)(2 + 2\nu)} \tag{5}$$

with $\nu = 1$ for SL and $\nu = 0.5$ for SB, x is the weight fraction of crystalline material, M and M_r are respectively the molecular weights of the chain and of the elementary incorporated rod, and $(\bar{l}^2)^{1/2}$ is the reentry length corresponding to the distance between two consecutive rods belonging to the same chain. In the term $\bar{r}_e^2$, the length

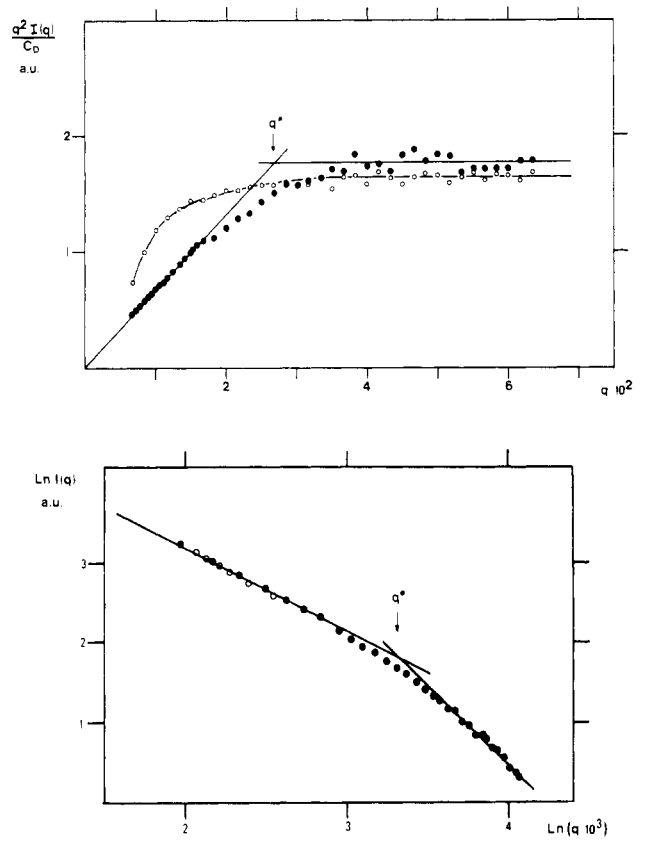

Figure 6. (a, top) Kratky plot $q^2I(q)$ vs. q. Full and opened circles correspond respectively to single crystal and amorphous samples. In both cases $M_{wIPSD} = 5 \times 10^5$. For $q < q^*$, $I(q) \sim q^{-1}$, and for $q > q^*$, $I(q) \sim q^{-2}$. (b, bottom) Log $I(q)$ vs. log q. The same results as previously plotted in a double logarithmic scale. The slopes are $p = 1$ for $q < q^*$ and $p = 2$ for $q > q^*$. Opened circles correspond to values obtained at D11 for the highest angles.

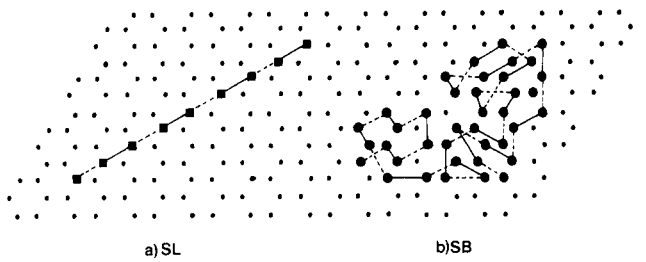

Figure 7. Schematic representation of the sheet-like incorporation (a) and the switch-board trajectory (b). Dotted lines and full lines stand for loops situated above and under the monocrystal, respectively.

l_c of the rod (i.e., lamella thickness) as well as the dimensions of the amorphous loops are taken into account. For Gaussian-like loops with an actual end-to-end distance I, we obtained

$$\bar{r}_e^2 = (3 - 2x)\frac{l_c^2}{12} + 2(1 - x)\bar{r}_B^2 + (2x + 1)\frac{I^2}{6} \quad (6)$$

where $\bar{r}_B^2$ is the radius of gyration of a loop calculated according to

$$\bar{r}_B^2 = 1/12(n\bar{b}^2 + I^2) \quad (7)$$

for which $n\bar{b}^2/6$ is the radius of gyration of the free equivalent Gaussian coil. In the case of IPS, only the first term of relation[6] is significant.

It appears immediately that our experimental result $\nu = 0.91$ agrees with the sheet-like model. To obtain such an increase of R_g particularly for the tagged chains of highest molecular weight and to fit the experimental results, we are led to perform the calculations of (5) with $(\bar{I}^2)^{1/2} = 12.6$ Å. This implies that the reentry does not occur between first neighbors ($(\bar{I}^2)^{1/2} = 7.3$ Å) but between second neighbors ($(\bar{I}^2)^{1/2} = 12.6$ Å). The theoretical difference in mean dimensions is sufficiently large to be sure of this point as it has been discussed elsewhere.[16] The other consequence is that reentrance occurs along planes containing stems of the same helicity. This certainly arises, as it has been emphasized in the case of bulk-crystallized experiments on IPS,[3,16] from the high energy ($\Delta E \sim 10$ kcal) required for the chain to change the configuration from a left to a right hand helix or vice versa. The small discrepancy observed with respect to the theoretical plot calculated after the experimental values of l_c and x certainly arises from unremoved or small pendant amorphous chains. Furthermore, as has been shown elsewhere,[16] the SB model provides for the IPS system values of ν that are mostly smaller than 0.5 in the range of molecular weights considered.

If the sheet-like incorporation model seems from the evolution of mean dimensions more appropriate, information provided at high q should allow clear-cut conclusions to be made.

The results obtained in the asymptotic domain can be examined by considering an expression for the form factor $P_s(q)$ of a thin sheet derived by Porod[17]

$$P_s(q) = \frac{2}{qL_c}\left[\frac{\pi'}{ql_c}\left(\int_0^{ql_c}\frac{J_1(x)}{x}\,dx\right) + \frac{1}{qL_c}\left(\frac{\sin(ql_c/2)}{(ql_c/2)}\right)^2 - \frac{\sin qL_c}{(qL_c)^2}\right] \quad (8)$$

where l_c and L_c are respectively the width and the length of the thin sheet and π' is a complex function reaching rapidly the value $\pi = 3.14$ just beyond the Guinier regime. For $qR_g >> 1$ two regions can be observed, $qL_c >> 1$ with $ql_c \ll 1$. Developing the Bessel function and neglecting the last two terms in relation 8 one obtains

$$P_s(q) \sim \frac{\pi}{qL_c}e^{-q^2l_c^2/24} \quad (9)$$

$qL_c \gg 1$ and $ql_c \gg 1$; then expression 8 reduces to the well-known result

$$P_s(q) \sim \frac{2\pi}{l_cL_cq^2} \quad (10)$$

At this stage of the discussion on the asymptotic behavior, it would be meaningless to regard the conformation involved in IPS single crystals as a pure thin sheet without taking into consideration the effect of amorphous loops. If they are characterized by a mean dimension $(\bar{r}_B^2)^{1/2}$, then the conformation can be considered sheet-like as far as $q(\bar{r}_B^2)^{1/2} \ll 1$ and the above relations are good approximations. A rough estimination of $(\bar{r}_B^2)^{1/2}$ from relation 7 or X-ray measurements for this case leads to

$$(\bar{r}_B^2)^{1/2} \sim 8\text{–}10 \text{ Å}$$

and therefore the results presented in this paper have always been obtained in the scattering vector domain q-$(\bar{r}_B^2)^{1/2} \ll 1$.

Returning to Figure 6, the Kratkyplot as well as the double logarithmic scale representation exhibit the two asymptotic behaviors defined by eq 9 and 10. From these behaviors the thickeness l_c of the lamellae can be deduced according to the two following ways: the value of q^* de-

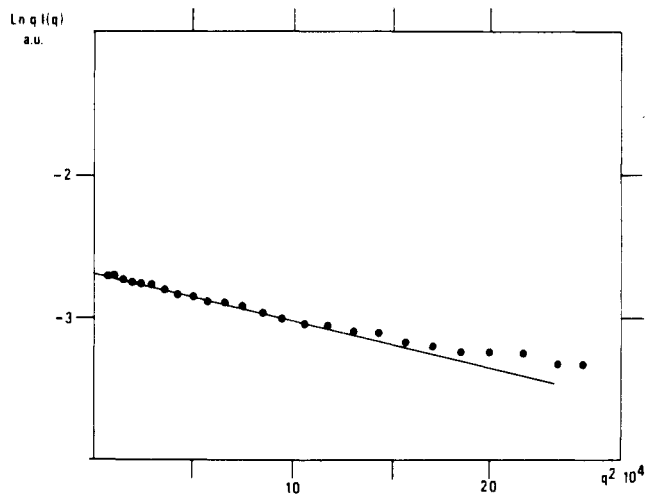

Figure 8. Log $[qI(q)]$ vs. q^2. The initial slope is directed related to the width of the sheet provided that the loops are small.

fined by the intercept of the asymptotes can be easily calculated leading to

$$l_c = 2/q^* = 75 \pm 4 \text{ Å} \quad (11)$$

and ploting log $qI(q)$ vs. q^2 in the first asymptotic domain, the value of the slope is directly related to l_c according to relation 9. Figure 8 shows such a plot for which one finds

$$l_c = 85 \pm 3 \text{ Å}$$

The values derived from SANS data are thus internally consistent and in good agreement with those found by electron microscopy and small-angle X-ray scattering.

Finally, a further result can be obtained from the Kratky plot. In a previous paper[3] we compared the ratio of the levels of the plateaus obtained in this representation between amorphous and crystalline samples containing the same tagged chains. In the case of interest here, ρ_{calcd} is deduced by considering the form factor for a thin sheet in the limit of large q

$$\rho_{calcd} = \frac{q^2 P_s(q)}{q^2 P_G(q)} = \frac{\pi R_G^2}{l_c L_C} \quad (12)$$

where R_G is the radius of gyration of the chains in the amorphous sample. Knowing $R_G = 185 \pm 10$ Å experimentally (Figure 5), and deducing $L_c = 1230$ Å from a mean value $l_c = 76$ Å and $x = 0.74$, one obtains

$$\rho_{calcd} = 1.15 \pm 0.12$$

Experimentally, as drawn in Figure 6a, we find $\rho_{exptl} = 1.06$, which is in quite good agreement with the theoretical derivation.

Conclusion

In this paper we confirm by SANS measurements the existence of the sheet-like model for chain incorporation in IPS single crystals grown from dilute solutions. The model is supported both by the variation of mean dimensions with molecular weight and by the short distance correlations. On the other hand, values of lamellar thickness l_c found by SANS, SAXS, and electron microscopy are in close agreement, showing the consistency of the data.

As mentioned in the introduction, the SANS single crystals study was the third step in the verification that the comparison between τ_m and τ_p can be a good criterion for deducing the conformation in the semicrystallized state. However, as has been emphasized in a recent Faraday discussion by Klein[18] and by Di Marzio et al.,[19] one has to take also into account the reptation or motion of the chain characterized by its translational diffusion coefficient D_T. Thus the comparison between τ_m and τ_p gives only a rough estimation of the conformation without predicting the exact number of rods in a regularly folded sequence.

Acknowledgment. The author wishes to thank Drs. B. Lotz and A Thierry for electron microscopy and X-ray measurements as well as Mrs. G. Pouyet for performing DSC thermograms.

References and Notes

(1) J. Schelten, D. G. H. Ballard, G. D. Wignall, G. Longman, and W. Schmatz, *Polymer*, **17**, 751 (1976).
(2) D. M. Sadler and A. Keller, *Macromolecules*, **10**, 1128 (1977).
(3) J. M. Guenet and C. Picot, *Polymer*, **20**, 1483 (1979).
(4) P. J. Flory and D. Y. Yoon, *Nature (London)*, **272**, 226 (1978).
(5) R. Suzuki, Thesis, Strasbourg, 1972.
(6) D. M. Sadler and A. Keller, *Polymer*, **17**, 37 (1976).
(7) M. D. Keith, R. G. Vadimsky, and F. J. Padden, *J. Polym. Sci., Part A-2*, **8**, 1687 (1970).
(8) G. Natta, *J. Polymn. Sci.*, **16**, 143 (1955).
(9) J. M. Guenet, Z. Gallot, C. Picot, and H. Benoit, *J. Appl. Polym. Sci.*, **21**, 2181 (1977).
(10) N. Overberg, M. Girolamo, and A. Keller, *J. Polym. Sci., Part A-2*, **15**, 1475 (1977).
(11) P. J. Lemstra, T. Kooistra, and G. Challa, *J. Polym. Sci., Part A-2*, **10**, 823 (1972).
(12) R. Dedeurwaerder and J. F. M. Oth, *J. Chem. Phys.*, **56**, 940 (1959).
(13) K. Ibel, *J. Appl. Crystallogr.*, **9**, 296 (1976).
(14) J. M. Guenet, C. Picot, and H. Benoit, *Macromolecules*, **12**, 868 (1979).
(15) B. Farnoux, M. Daoud, D. Decker, G. Jannink, and R. Ober, *J. Phys. (Paris), Lett.*, **36**, 35 (1975).
(16) J. M. Guenet and C. Picot, *Polymer*, **20**, 1473 (1979).
(17) G. Porod, *Kolloid Z.*, **124**, 83 (1951).
(18) J. Klein, *Faraday Discuss. Chem. Soc.*, in press.
(19) E. A. Di Marzio, C. M Guttman, and J. D. Hoffman, *Faraday Discuss. Chem. Soc.*, in press.